Quantum illumination using non-Gaussian states generated by photon subtraction and photon addition

Longfei Fan and M. Suhail Zubairy
Institute for Quantum Science and Engineering (IQSE) and Department of Physics & Astronomy, Texas A&M University, College Station, Texas 77843, USA

(Received 26 April 2018; published 17 July 2018)

Quantum illumination takes advantage of quantum entanglement to achieve low error probability for detecting a low reflective object embedded in a noisy thermal bath. The two-mode squeezed state (TMSS), which is a Gaussian state, has been applied to quantum illumination as the detecting states in experiment. The photon-subtracted TMSS has also been proposed to achieve even lower error probability. Here we study quantum illumination with non-Gaussian states generated by photon subtraction and photon addition. Helstrom limit and quantum Chernoff bound are evaluated for comparison between performance of states with the same squeezing strength and with the same signal strength, respectively. Particularly, states generated by asymmetrical coherent superposition of photon subtraction and addition are studied, which are shown by us to have better performance than symmetrical ones. We show that non-Gaussian operations enhance the quantum illumination by introducing both stronger entanglement and signal strength. We then give a strategy on how to choose the optimal states for the best performance in different scenarios.

DOI: 10.1103/PhysRevA.98.012319

I. INTRODUCTION

Quantum illumination [1,2], also called entanglement-enhanced sensing, utilizes entangled states to enhance the performance of a target-detection task in a lossy and noisy scenario. Unlike other entanglement-assisted quantum techniques, it can still benefit from entanglement in an entanglement-breaking environment [1–3]. Gaussian quantum illumination using two-mode squeezed states (TMSS) has been proposed [4] and realized experimentally [5–8]. Quantum illumination has inspired applications in quantum security communication [9,10], microwave quantum radar [11], and cloaking [12]. The measurement step of quantum illumination can be regarded as a binary quantum state discrimination task [13–16], whose performance is evaluated by detection error probability [17–20]. Besides, quantum illumination can be studied in the context of quantum hypothesis testing [21], quantum estimation [22], and quantum communication protocol [23,24]. It is also one kind of quantum imaging [25].

Non-Gaussian quantum resources play important roles in quantum information [26]. Photon subtraction and photon addition can generate non-Gaussian states with enhanced entanglement and quantum correlation [27–29]. Entanglement is regarded as the key resource assisting quantum illumination [1,2,4]. It has been shown that a photon-subtracted TMSS achieves lower error probability [30], where the detecting states compared have the same squeezing strength. Coherent superposition of photon subtraction and addition can enhance entanglement more than mere subtraction and addition, particularly in small squeezing regimes [31,32], in which quantum illumination also has the most advantages [1,2,4]. Thus we could expect coherent superposition of photon subtraction and addition can enhance quantum illumination more than other non-Gaussian operations.

Even though entanglement is regarded as the key resource for quantum illumination, mutual information and quantum discord [33,34] have also been shown to be sources assisting quantum illumination [23,24,35]. The fractional increase of mutual information is shown to give a close approximation of signal-to-noise ratios [35]. Quantum discord explains the resilience of quantum illumination in entanglement-breaking channels [23,24]. Here we only use entanglement as an indicator of performance. We show that comparison between entanglement strength of states gives us useful clues on how to choose better detecting states for quantum illumination.

In this paper, we apply various two-mode entangled states to quantum illumination, including the non-Gaussian states obtained by photon subtraction and photon addition. We then study the error probability of each state with respect to its squeezing strength and signal strength. The performance is evaluated using the Helstrom limit [13] and the quantum Chernoff bound [17]. The entanglement strength of the detecting state is measured by entropy of entanglement. We show that under the same squeezing strength, non-Gaussian states can enhance quantum illumination because of their larger entanglement and signal strength. However, the TMSS performs better than other non-Gaussian states when a constraint on signal strength is applied. We also show that the asymmetrical coherent superposition of photon subtraction and addition can achieve better performance than symmetrical ones.

This article is organized as follows. In Sec. II A, we give a brief review of quantum illumination and its equivalent model. In Sec. II B, we introduce various non-Gaussian states and discuss their properties on entanglement and signal strength. In Sec. III A we compare the performance of these states under the same squeezing strength. In Sec. III B, we make a comparison between performances of states under the same

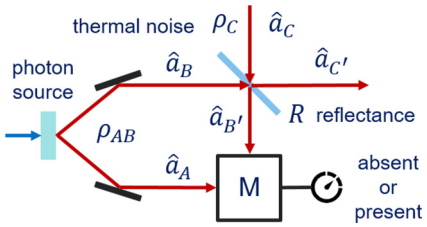

FIG. 1. Model of quantum illumination.

signal strength. In Sec. IV, we study the performance of asymmetrical two-mode entangled states.

II. QUANTUM ILLUMINATION AND NON-GAUSSIAN STATES

A. Quantum illumination

The task of quantum illumination is to determine the existence of a low-reflective object which is embedded in a noisy thermal bath. Its equivalent model is illustrated in Fig. 1. The two-mode entangled photon state $\rho_{\rm AB}$ is used as the detecting state. The mode B (signal) is sent for detecting the suspect object; i.e., it can be reflected back by the object if there exists one. The mode A (idler) is retained to be measured together with the returned signal B'. The suspect object can be modeled by a beam splitter with low reflectance R. The thermal noise C, whose average photon number is $N_{\rm th}$, will enter the final measurement device M if no object is present. If an object is present, the thermal noise is mixed with B by the beam splitter. In the latter case, the average photon number of the thermal noise is adjusted to be $N'_{\rm th} = \frac{N_{\rm th}}{1-R}$ during numerical calculation to compensate for the loss during mixing.

Let the photon annihilation operators for the idler, the signal, and the thermal noise be a_A, a_B, and a_C. The two-mode mixing operator $U(\xi) = \exp(\xi a_B^\dagger a_C - \xi^* a_B a_C^\dagger)$ describes the beam splitter, where $\xi = \arcsin\sqrt{R}$. The output modes after mixing are labeled by $a_{B'}$ and $a_{C'}$ as shown in Fig 1. Thus we have $a_{B'} = \cos(\xi)a_C - \sin(\xi)a_B$. Two possible output states ρ_0 and ρ_1 can enter the measurement device M, depending on whether the suspect object is absent or present:

$$\begin{aligned} &\text{absent (nomixing): } \rho_0 = \mathrm{Tr_B}[\rho_{\rm AB}] \otimes \rho_{\rm C}, \\ &\text{present (mixing): } \rho_1 = \mathrm{Tr_C}[\mathrm{U}\rho_{\rm AB} \otimes \rho_{\rm C}\mathrm{U}^\dagger]. \end{aligned} \tag{1}$$

Next step, we use a measurement device M to infer whether an object is present or not by discriminating above two states as best as we can. The performance of discrimination is measured by the error probability of inference, which may depend on *a priori* probability. Here we assume that the suspect object is equally absent and present. When we have N identical copies of entangled states for detection, the optimal error probability is given by the Helstrom limit [13]:

$$P_{{\rm err},N} = \tfrac{1}{2}\big(1 - \tfrac{1}{2}\big|\big|\rho_0^{\otimes N} - \rho_1^{\otimes N}\big|\big|\big). \tag{2}$$

It is difficult to evaluate because of the high dimensionality. Another difficulty is that it is not monotonic for the tensor power. An asymptotically tight upper bound, which is called the quantum Chernoff bound (QCB) [17], is easier to evaluate and is given by

$$P_{{\rm err},N} \leqslant \tfrac{1}{2}P_{\rm QCB}^N = \tfrac{1}{2}\left\{\min_{0\leqslant t\leqslant 1} \mathrm{Tr}\big[\rho_0^{\rm t}\rho_1^{1-{\rm t}}\big]\right\}^N. \tag{3}$$

We use the above two quantities to measure the performance of quantum illumination. Meantime the entanglement of a detecting state can be measured by the von Neumann entropy of reduced density operators, which is given by

$$E(|\psi_{\rm AB}\rangle) = -\mathrm{Tr}[\rho_{\rm A}\ln\rho_{\rm A}] = -\mathrm{Tr}[\rho_{\rm B}\ln\rho_{\rm B}], \tag{4}$$

where $\rho_{\rm A} = \mathrm{Tr_B}|\psi_{\rm AB}\rangle\langle\psi_{\rm AB}|$ and $\rho_{\rm B} = \mathrm{Tr_A}|\psi_{\rm AB}\rangle\langle\psi_{\rm AB}|$. We call it the "entropy of entanglement" and use the label E for it hereafter.

B. Non-Gaussian entangled states

The TMSS is a widely used entanglement state in continuous-variable quantum information [36,37]. It is given by

$$|\mathrm{TMSS}\rangle = \sqrt{1-\lambda^2}\sum_{n=0}^{\infty}\lambda^n|n\rangle|n\rangle, \tag{5}$$

where $\lambda = \tanh s$ and s is the squeezing parameter. The TMSS is a Gaussian state. Quantum illumination has been realized experimentally with the TMSS as the entangled detecting photon source [4–8]. As entanglement is regarded as the key quantum resource assisting quantum illumination, we expect that detecting states with enhanced entanglement strength can achieve lower error probability.

A combination of photon-subtraction and photon-addition operations can generate various non-Gaussian entangled states which have enhanced entanglement [27,28]. Here we study states obtained by following non-Gaussian operations: photon-subtraction (PS), photon-addition (PA), photon-subtraction-following-addition (PSA), and photon-addition-following-subtraction (PAS). It has also been shown that a coherent superposition of both photon subtraction and photon addition [31] leads to the strongest enhancement of entanglement under small squeezing strength [32]. We call the non-Gaussian state generated by such an operation a "PCS" state for short. The former four kinds of states are given by

$$\begin{aligned} \hat{a}\hat{b}|\mathrm{TMSS}\rangle &\doteq \sqrt{A_1}\sum_{n=0}^{\infty}(n+1)\lambda^n|n\rangle|n\rangle, \\ \hat{a}^\dagger\hat{b}^\dagger|\mathrm{TMSS}\rangle &\doteq \sqrt{A_1}\sum_{n=0}^{\infty}(n+1)\lambda^n|n+1\rangle|n+1\rangle, \\ \hat{a}\hat{a}^\dagger\hat{b}\hat{b}^\dagger|\mathrm{TMSS}\rangle &\doteq \sqrt{A_2}\sum_{n=0}^{\infty}(n+1)^2\lambda^n|n\rangle|n\rangle, \\ \hat{a}^\dagger\hat{a}\hat{b}^\dagger\hat{b}|\mathrm{TMSS}\rangle &\doteq \sqrt{A_2}\sum_{n=0}^{\infty}(n+1)^2\lambda^n|n+1\rangle|n+1\rangle, \end{aligned} \tag{6}$$

where the $\doteq$ means that the left-hand side equals the right-hand side after normalization. The normalization factors are given by

$$A_1 = \frac{(1-\lambda^2)^3}{1+\lambda^2}, \quad A_2 = \frac{(1-\lambda^2)^5}{1+11\lambda^2+11\lambda^4+\lambda^6}. \tag{7}$$

The PCS state is given by [32]

$$\begin{aligned}(t_a\hat{a}+r_a\hat{a}^\dagger)(t_b\hat{b}+r_b\hat{b}^\dagger)|\mathrm{TMSS}\rangle \\ \doteq \sqrt{A_3}\sum_{n=0}^{\infty}\lambda^n[\lambda t_a t_b(n+1)|n\rangle|n\rangle \\ +\lambda t_a r_b\sqrt{(n+1)(n+2)}|n\rangle|n+2\rangle \\ +\lambda r_a t_b\sqrt{(n+1)(n+2)}|n+2\rangle|n\rangle \\ +r_a r_b(n+1)|n+1\rangle|n+1\rangle], \end{aligned} \tag{8}$$

where $t_i^2+r_i^2=1(i=a,b)$, and the normalization factor is given by

$$A_3=\frac{(1-\lambda^2)^3}{\lambda^2(1+|t_a r_b^*+r_a t_b^*|)+|t_a t_b\lambda^2+r_a r_b|^2}. \tag{9}$$

Some properties of these non-Gaussian states have been discussed in previous studies [28,32]. However, the previous discussion on PCS states is limited to symmetrical ones, where $r_a=r_b$ holds. Here we show properties of these states with a focus on their entanglement and photon numbers, particularly for asymmetrical PCS states. We illustrate the entropy of entanglement E in Fig. 2(a) and the total average photon number $\langle n\rangle$ in Fig. 2(b) for each state with respect to λ. The ratio between them, which indicates entanglement provided by each photon, is illustrated in Fig. 2(c). It is shown that for a given λ, PS and PA have the same entropy of entanglement E; however, PA has one more photon per mode than that of PS. Similar results are observed for PSA and PAS. Meanwhile PSA (PAS) has larger entanglement than PS (PA). Therefore, non-Gaussian operations not only enhance entanglement, but also bring larger average photon numbers, i.e., signal strength.

The properties of PCS are somehow complicated because of free choices on r_a and r_b. In Fig. 2, for each λ, we choose the pair of r_a and r_b which leads to the largest entropy of entanglement E for plotting. With such choices, the PCS state has the most enhanced entanglement of any other state under small squeezing strength for $\lambda\lessapprox 0.15$. In the region from $\lambda\approx 0.15$ to $\lambda\approx 0.35$, its entanglement becomes less than that of PAS and PSA, but it is still larger than the entanglement of other states. When $\lambda\gtrapprox 0.35$, the optimal PCS reduces to PA or PS. That is to say, there are two optimal choices which lead to the largest entanglement: $r_a=r_b=0$ and $r_a=r_b=1$. In Fig. 2(b), the curve of PCS starts from point (0,1.0), and then it goes between the curves of PS and PA until the point around $\lambda=0.05$. For λ from 0.05 to 0.35, the curve of PCS almost overlaps with that of PA ($r_a=r_b=1$). Our numerical results show that values of r_a and r_b are very close to 1.0, but not identical to 1.0. For $\lambda\gtrapprox 0.35$, the optimal PCS reduces to either PA or PS as mentioned earlier. In the plot, we choose to set $r_a=r_b=1$, so the curve of PCS overlaps exactly with that of PA for $\lambda\gtrapprox 0.35$.

It would be a practical consideration to achieve better detecting performance with less photons consumed. To get some clues, we plot entanglement provided per photon $E/\langle n\rangle$ with respect to λ in Fig. 2(c) for all these states. It is shown that the TMSS is the most "efficient" one to obtain entanglement with the least number of photons. We could expect that the TMSS would perform best for quantum illumination if we have a constraint on signal strength. The PA, PAS, and PCS

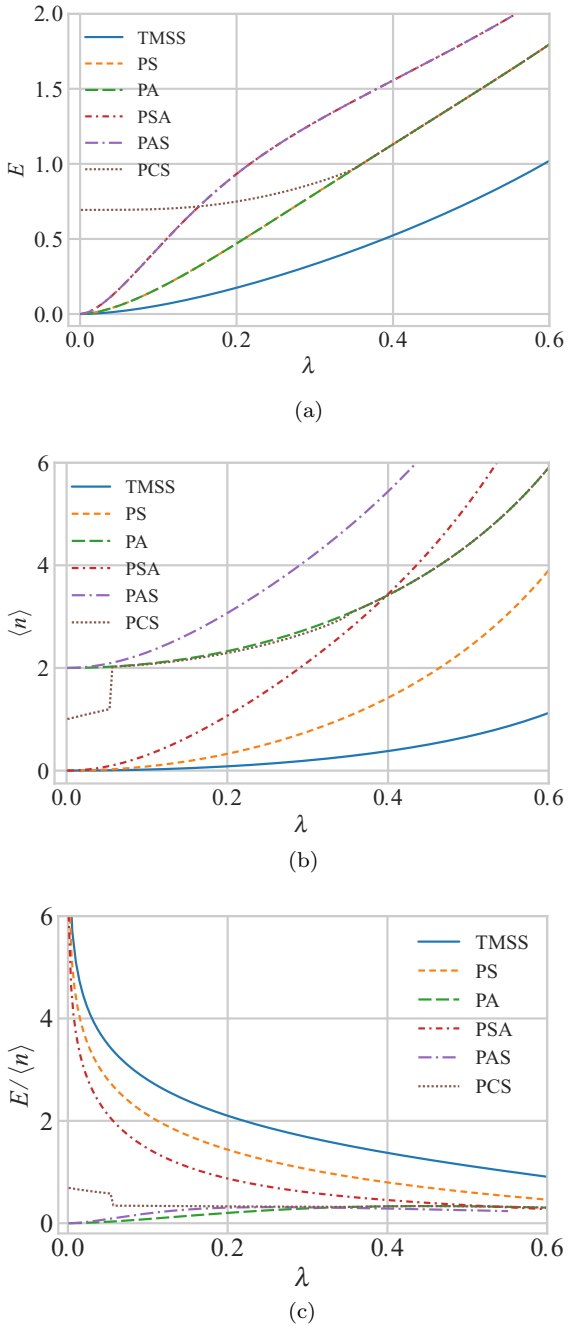

FIG. 2. (a) Entropy of entanglement E, (b) signal strength $\langle n\rangle$, and (c) entanglement provided per photon $E\ \langle n\rangle$, for TMSS and non-Gaussian states under given values of λ ranging from 0.0 to 0.6. (a) Comparison of entanglement E among states with respect to λ. Here we have extra notes for PCS states. As a PCS state is determined by the three variables r_a, r_b, and λ, its entanglement still varies with respect to r_a and r_b when λ is given. In the plot above, the curve of PCS states shows the maximum E can be obtained for each λ; i.e., the optimal pairs of r_a and r_b for each λ are used for calculating the E of PCS states. (b) Comparison of average photon numbers $\langle n\rangle$ among states with respect to λ. The values of r_a and r_b used for PCS states for each given λ are the same as those used in panel (a). So the $\langle n\rangle$ of PCS shown in the curve may not be the maximum one for each λ. (c) Comparison of $E/\langle n\rangle$ among states with respect to λ. The values of r_a and r_b used for PCS states for each λ are the same as those used in panel (a).

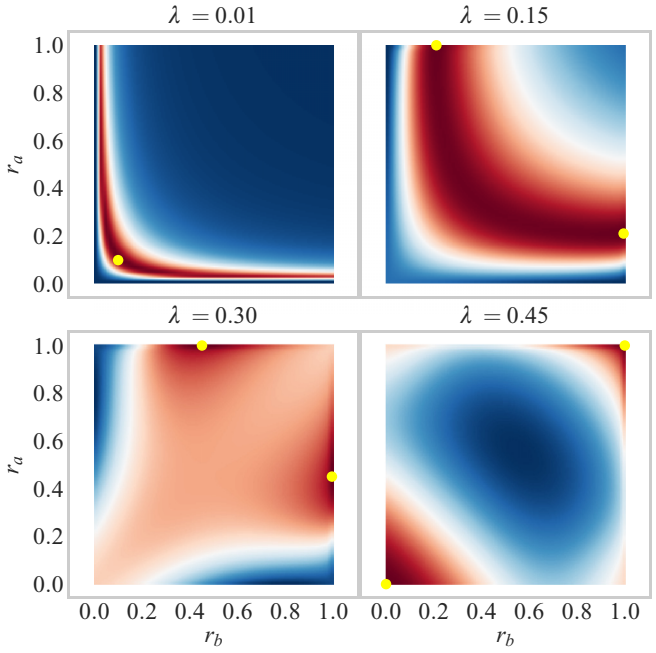

FIG. 3. Entropy of entanglement E with respect to r_a and r_b for PCS states given for four different values of λ. All four subplots are symmetrical with respect to $r_a = r_b$. Optimal points which have the largest entanglement have been labeled in each plot by solid yellow dots. They are (0.100,0.100) for λ = 0.01, (0.211,1.00) and (1.00,0.211) for λ = 0.15, (0.451,1.00) and (1.00,0.451) for λ = 0.30, and (0.0,0.0) and (1.0,1.0) for λ = 0.45.

states are less "efficient" as their photon-addition operations increase their average photon numbers a lot, meanwhile their entanglement is not enhanced that much.

PCS states show complicated curves, as they have free choices on r_a and r_b. Four examples to show how their entanglement depends on r_a and r_b are illustrated in Fig. 3. It is obvious that the modes A and B are equivalent so that the plots are symmetrical around the antidiagonal line where $r_a = r_b$ holds. Numerical results show that for $\lambda \lessapprox 0.05$, the optimal choices to obtain the largest entanglement are symmetrical states so that $r_a^{\text{opt}} = r_b^{\text{opt}}$. Then the optimal points move to the edge as λ increases, i.e., $r_a = 1$ or $r_b = 1$. Finally the optimal points move to and stay on two antidiagonal vertices.

III. COMPARISON OF PERFORMANCE

The photon subtracted two-mode squeezed state has been compared with the TMSS for quantum illumination [30]. The comparison between these two kind of states was made under the condition that they have the same squeezing strength, i.e., the same λ. Here we extend the comparison to all non-Gaussian states mentioned in Eqs. (6) and (8). We carry out numerical calculations of the quantum Chernoff bound and the Helstrom limit for $N = 1$ using Eqs. (2) and (3) to evaluate the performance. We first make a comparison of performance under the same squeezing strength in Sec. III A like what has been done in the Ref. [30]. Then, in Sec. III B we make a comparison under the signal strength of mode B, i.e., the same average photon number $\langle n_B \rangle$ of mode B.

Setup. As mentioned in Ref. [1,4], quantum illumination shows its greatest advantage under low signal-to-noise ratios. Also it has to be mentioned that these two-mode states approach classical-state behavior when their signal strength is too large [4]. Therefore, throughout our numerical calculations, we set up the low-reflectance and high-noise scenario. The reflectance of suspect object $R = 0.01$. The average photon number of thermal noise has a relatively large value so that $N_{\text{th}} = 1.0$. Values of λ are also limited to be below 0.6 in order to keep the signal strength of detection states small enough. In such a scenario, error probability for detection using one copy of state is close to 0.5, as the signal is too weak to distinguish between two possible output states.

Methods. We use PYTHON, NUMPY, SCIPY, and the QUTIP [38,39] quantum toolbox for numerical calculations. MATPLOTLIB and SEABORN are used for plotting figures. In QUTIP, a Fock state $|n\rangle$ is created by `basis(n_max, n)`, where `n` is the Fock number and `n_max` is the truncated photon numbers for numerical calculation. We set `n_max` = 32 throughout our numerical simulations. First, we create all these two-mode states shown in Eqs. (5), (6), and (8) by summation of the tensor product of Fock states over n from $n = 0$ to $n = 31$. For example we can create a TMSS by `tmss = sum([lambda ** n * tensor(basis(n_max, n), basis(n_max, n)) for n in range(n_max)]).unit()`, where `.unit()` is a normalization operation. The annihilation operator `a = destroy(n_max)`, then the two-mode mixing operator $U(\xi) = \exp(\xi a_B^\dagger a_C - \xi^* a_B a_C^\dagger)$ can be created by `U = s * tensor(a.dag(), a) - conj(s) * tensor(a, a.dag())`. With these density matrix and operators created, we can obtain ρ_0 and ρ_1 shown in Eq. (1), and the Helstrom limit shown in Eq. (2). The calculation can be carried out straightforwardly using methods of tensor product, partial trace, and trace norm, which are predefined in the QUTIP toolbox. The numerical calculation of the quantum Chernoff bound takes some extra effort as optimal t needs to be found. It is fulfilled by using the `minimize` method from `scipy.optimize`.

A. Under the same squeezing strength

Here we first study how performance changes with respect to λ for each state. Then we compare the performance of these states given the the same λ. The results for the quantum Chernoff bound and the Helstrom limit are illustrated in Figs. 4(a) and 4(b), respectively. The two figures show similar results and conclusions. First we discuss the states except the PCS state. The rank of performance, from the best to the worst, is in the order of PAS, PSA, PA, PS, and TMSS. The ranking order can be understood by looking at Fig. 2. For a given value of λ, PSA and PAS have the most enhanced entanglement, then PS and PA follow. The TMSS has the smallest entropy of entanglement. Meanwhile PAS (PA) has a larger signal strength than PSA (PS). As both the entanglement strength and the signal strength affect the performance, this explains why we get the ranking order mentioned above.

In Fig. 4, we plot two curves for PCS states, labeled by PCS-etgl and PCS-opt, respectively. For the curve of PCS-etgl, we choose those r_a and r_b which lead to the largest

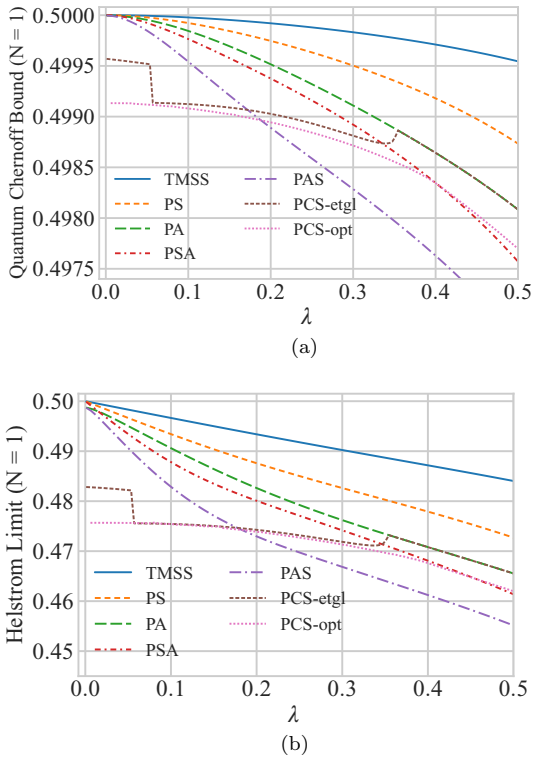

FIG. 4. (a) Quantum Chernoff bound and (b) Helstrom limit with respect to λ for quantum illumination using a single copy of the detecting state ($N = 1$). Here we set $N_{\text{th}} = 1.0$ and $R = 0.01$. Here we have some extra notes for PCS states. Two curves for PCS states are plotted in both panels (a) and (b). The points for the curve of PCS-etgl are constituted with PCS states which have the largest entanglement under a given λ, i.e., the r_a and r_b used here are the same as what we used for plotting Fig. 2(a). Meanwhile, the curve of PCS-opt shows the optimal lowest quantum Chernoff bound which a PCS state can reach for each λ.

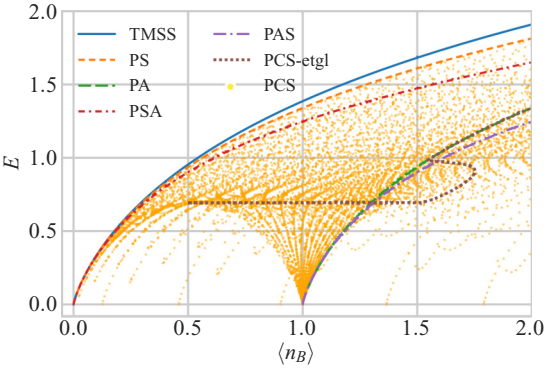

FIG. 5. Entropy of entanglement E vs average photon number $\langle n_B \rangle$ of mode B. r_a and r_b are sampled for PCS states to make scattered plots. The TMSS has the largest entropy of entanglement among these states when they all have the same $\langle n_B \rangle$. The points of the PCS states are bounded by the curve of PS from the top. (Notice that states used for plotting PCS-etlg are optimized for each λ; they are no longer the optimal states with the largest entanglement for each $\langle n_B \rangle$. For the same $\langle n_B \rangle$, PCS states can have different combinations of r_a, r_b, and λ, so we observe the u-turn shape of the PCS-etgl curve around $\langle n_B \rangle = 1.6$.)

entanglement as in Fig. 2. Meanwhile the PCS-opt curve shows the lowest error probability a PCS state can achieve for each λ. In the region where λ is smaller than about 0.17, the PCS state outperforms all other states, which results from its advantage in both entanglement and signal strength as shown in Fig. 2. We find similar stairs jumping at about the same positions ($\lambda \approx 0.05$) in both Figs. 4 and 2(b), which indicates the signal strength has an impact on the performance.

The deviation between curves of PCS-etgl and PCS-opt also shows that entanglement is not the only factor determining the performance of quantum illumination. The choices of r_a and r_b which result in the largest entanglement do not always lead to the lowest quantum Chernoff bound, because the signal strength also matters. Here is an example for the case where $\lambda = 0.0995$ (such that we have $\langle n_B \rangle = 0.01$ for the TMSS), $N_{\text{th}} = 1.0$, and $R = 0.01$. The optimal points which have the largest entanglement are (0.140,1.0) (A) and (1.0,0.140) (B). The corresponding quantum Chernoff bounds are 0.499 124 and 0.499 550 respectively. Meanwhile, the lowest quantum Chernoff bound can be achieved under the same λ is 0.499 081, which is obtained at point C (0.118,0.950). It is very close to point A, which has the maximum entanglement. Point C has entanglement of 0.688 and $\langle n_B \rangle$ of 1.544. Meanwhile point A has entanglement of 0.699 and $\langle n_B \rangle$ of 1.529. Even though point C has less entanglement strength, it has larger signal strength. The overall effect makes point C achieve the lowest quantum Chernoff bound.

In summary, suppose now we have a TMSS in the laboratory, we could further improve the performance of quantum illumination by applying various non-Gaussian operations on it, as such operation can enhance the entanglement and the signal strength of the detecting states at the same time. Among all these non-Gaussian states, the PCS state performs the best under small squeezing strength, as it can enhance the entanglement the most.

B. Under the same signal strength

From Fig. 2 we learn that non-Gaussian operations on the TMSS will not only enhance entanglement, but also bring larger average photon numbers. Both factors can enhance the performance of quantum illumination. The former is a quantum effect, while the latter is purely classical. Furthermore, in practice we would like to achieve the same performance with less power, particularly with less power of mode B, as a large detecting signal can also be detected by the other party we would like to detect, which exposes ourselves. Since mode B is sent out for detection, a constraint on its signal strength could be a practical consideration.

As entanglement is the key resource of quantum illumination, we first explore how the entropy of entanglement E varies with respect to different states under the same signal strength of mode B. The results are shown in Fig. 5. We find that the TMSS has the largest E of any other states under the same $\langle n_B \rangle$. PCS states can have different values of E even for the same $\langle n_B \rangle$ because of the free choices of r_a and r_b, so we show points of PCS states with scatter plots. An upper boundary of all possible PCS points is observed, which exactly overlap

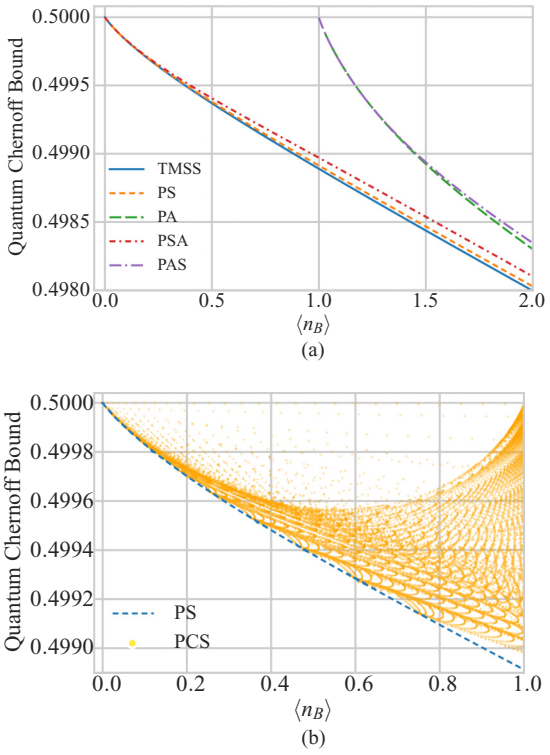

FIG. 6. Quantum Chernoff bounds with respect to the signal strength, i.e., the average photon number $\langle n_B \rangle$ of mode B. (a) In this figure, we compare Quantum Chernoff bounds among states except the PCS states under the same signal strength, i.e., the same average photon number $\langle n_B \rangle$ of mode B. It is shown that given the same $\langle n_B \rangle$, detecting using the TMSS can get the lowest quantum Chernoff bound. (b) Here we show quantum Chernoff bounds of PCS states with respect to the signal strength. Again we sample r_a and r_b to plot scattered points. It is shown that these scattered points of PCS states are bounded by the curve of PS states from the bottom, which is a counterpart for the upper boundary shown in Fig. 5.

with the curve of PS. Therefore, given an arbitrary value of $\langle n_B \rangle$, the optimally chosen PCS state can only perform as well as a PS state with the same $\langle n_B \rangle$. No PCS state can achieve larger E than the TMSS. The states constituting the PCS-etgl curve in Fig. 5 are the same as what we use in Fig. 2. It is far below the upper boundary. Since their r_a and r_b are optimized for each λ, they are no longer the optimal choices for a given $\langle n_B \rangle$. Given the same $\langle n_B \rangle$, the optimal PCS state which has the largest entanglement reduces to a PS state.

The above results for E vs $\langle n_B \rangle$ give us some clues on the strategy of how to choose the optimal detecting state. We would choose the TMSS, as it has the largest entanglement for each $\langle n_B \rangle$. We illustrate in Fig. 6 how the quantum Chernoff bound changes with respect to $\langle n_B \rangle$ to show that our strategy is correct. The TMSS achieves the lowest quantum Chernoff bound among these states under the same $\langle n_B \rangle$. Then PS and PSA follow. PA and PAS fall far behind, particularly for $\langle n_B \rangle < 1$. Their minimum $\langle n_B \rangle$ is 1.0, meanwhile the curves of other states start from (0.0,0.5). In Fig. 6(b), PCS states with different values of r_a and r_b are sampled and shown with scatter plots. It is clearly seen that these scatter points are bounded by the curve of PS like what we have observed in Fig. 5. So under the same $\langle n_B \rangle$, the optimal PCS state which achieves the lowest quantum Chernoff bound reduces to a PS state. The results shown here are rather different from the results shown in Fig. 4, where comparisons are made given the same squeezing strength λ. We get a ranking order reversed from that in Sec. III A.

So the strategy of choosing optimal states for detecting depends on what constraints we have on states. First if we can choose detecting states freely, the TMSS is the optimal one, whenever there is a constraint on squeezing strength or signal strength. If there is a constraint on the signal strength of mode B, the TMSS can achieve the lowest quantum Chernoff bound for a given value of $\langle n_B \rangle$ as shown in Fig. 6(a). Meanwhile if there is no constraint on the signal strength of mode B, the TMSS is still the one that costs the least detecting power to obtain an equal quantum Chernoff bound. Second assume that we have limited TMSS sources available in our laboratory, we could consider applying additional non-Gaussian operations on these TMSS sources to obtain better performance.

It can be seen that Fig. 6(a) is like a mirroring of Fig. 5 with respect to the x axis. Also, Fig. 4(a) is like a mirroring of Fig. 2(a). Both Figs. 5 and 2(b) show how entanglement changes. This again indicates qualitatively that entanglement is the key quantum resource assisting quantum illumination. Form the curves of entanglement, we can get some clues on how well states perform in quantum illumination.

IV. ASYMMETRICAL PCS STATES

We have mentioned in Sec. III A that the PCS states which have the largest entanglement for λ do not always result in the best performance for the same λ. Here we show an example to explain the reason behind this. First, we notice that the model of quantum illumination shown in Fig. 1 is asymmetrical, because the signal mode B and the idler mode A go through rather different channels. Second, recall that the PCS states can have asymmetrical operations on the two modes, respectively, as

$$\mathrm{PCS} = \sqrt{N_3}(t_a\hat{a} + r_a\hat{a}^\dagger)(t_b\hat{b} + r_b\hat{b}^\dagger)|\mathrm{TMSS}\rangle. \tag{10}$$

By setting unequal values for r_a and r_b, we get asymmetrical PCS states. One aspect of asymmetry is that two modes can have different average photon numbers. We show how the average photon numbers of two modes change with respect to r_a and r_b in Fig. 7, where we set $\lambda = 0.0995$. It is not strange that each mode achieves the largest average photon number if its coefficient $r_i (i = a,b)$ for the creation operator is 1.0. As mode B is sent out for detection, it must be large enough to resist noise.

An example is illustrated in Fig. 8 to show how entanglement and signal strength affect the performance of quantum illumination with PCS states. The parameters we set are $N_{\mathrm{th}} = 1.0$, $R = 0.01$, and $\lambda = 0.0995$. The entropy of entanglement E is symmetrical with respect to the antidiagonal, where $r_a = r_b$. There is a symmetrical L-shaped dark red band, where the state has larger entropy of entanglement. However, the quantum Chernoff bound is not symmetrical about the antidiagonal. There is still an L-shaped band, which matches roughly the L-shaped band shown in Fig. 8(a). However, the optimal area which has the lower quantum Chernoff bound moves to the bottom right corner of the L-shaped band, where

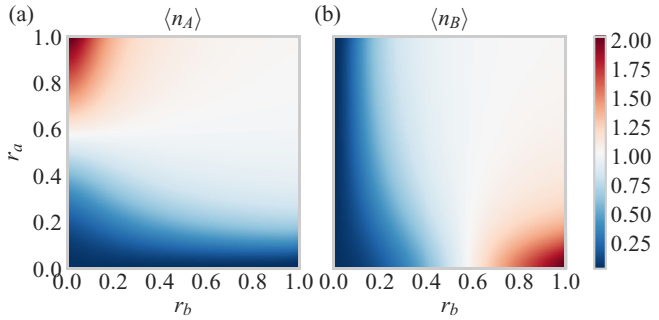

FIG. 7. Average photon numbers of each mode for PCS states with respect to r_a and r_b. (a) Average photon numbers $\langle n_A \rangle$ of mode A, which is retained in the laboratory. (b) Average photon numbers $\langle n_B \rangle$ of mode B, which is sent out for detection. Here we set $\lambda = 0.0995$ in both panels (a) and (b). For comparison, the TMSS with the same value of λ has an average photon number of 0.01 for each mode.

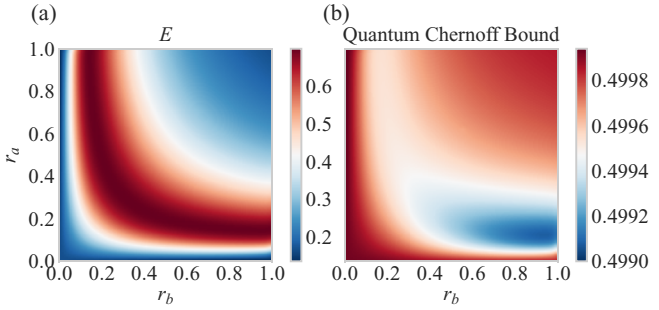

FIG. 8. (a) Entropy of entanglement for PCS states with respect to r_a and r_b. (b) Quantum Chernoff bound for PCS states with respect to r_a and r_b. In both panels (a) and (b), we set $N_{\text{th}} = 1.0$, $R = 0.01$, and $\lambda = 0.0995$.

$\langle n_B \rangle$ is larger as shown in Fig. 7. The results for the quantum Chernoff bound are as expected, because both the entanglement and the signal strength affect the performance of quantum illumination. Therefore when we use PCS states for quantum illumination, an asymmetrical one where $\langle n_B \rangle > \langle n_A \rangle$ will outperform symmetrical input states where $\langle n_B \rangle = \langle n_A \rangle$.

The results shown here again prove our conclusion that both the entanglement and the signal strength of the detecting state would affect the error probability of quantum illumination. From the quantum point of view, a larger amount of entanglement results in larger quantum correlations between two modes. From the classical point of view, stronger signals are less vulnerable to noisy and lossy environments.

V. CONCLUSION

In this article, we explored the performance of different two-mode entangled states for quantum illumination, including the TMSS and non-Gaussian states obtained by applying photon-subtraction and photon-addition operations to the TMSS. We evaluated the Helstrom limits and the quantum Chernoff bounds achieved by these states for comparisons given the same squeezing strength and the same signal strength, respectively. We also explored the performance of asymmetrical PCS states generated by an asymmetrical coherent superposition of both photon subtraction and photon addition.

In summary, we conclude that non-Gaussian operations can enhance the performance of quantum illumination compared with the base TMSS where we apply these operations. With these non-Gaussian operations, we obtain lower error probability by introducing both stronger entanglement and average photon numbers. Both factors affect the performance of quantum illumination, the former is a quantum effect, and the latter is a classical effect. However, if the signal strength must be constrained, the TMSS is the best choice. It delivers the same performance with the least number of photons consumed. When choosing the PCS state as the detecting state, we would consider an asymmetrical configuration to achieve lower error probability by making the signal (mode B) stronger than the idler (mode A). It is also possible to make many other kinds of asymmetrical non-Gaussian states besides PCS states, for example, by two photon-subtraction operations on one mode and just one photon-addition operation on the other mode. The asymmetrical properties of the quantum illumination channel need further study to find the optimal detecting states.

ACKNOWLEDGMENTS

This research is supported by NPRP Grant No. 8-751-1-157 by the Qatar National Research Fund (QNRF).

[1] S. Lloyd, Science **321**, 1463 (2008).
[2] J. H. Shapiro and S. Lloyd, New J. Phys. **11**, 063045 (2009).
[3] M. F. Sacchi, Phys. Rev. A **72**, 014305 (2005).
[4] S.-H. Tan, B. I. Erkmen, V. Giovannetti, S. Guha, S. Lloyd, L. Maccone, S. Pirandola, and J. H. Shapiro, Phys. Rev. Lett. **101**, 253601 (2008).
[5] S. Guha and B. I. Erkmen, Phys. Rev. A **80**, 052310 (2009).
[6] E. D. Lopaeva, I. Ruo Berchera, I. P. Degiovanni, S. Olivares, G. Brida, and M. Genovese, Phys. Rev. Lett. **110**, 153603 (2013).
[7] Z. Zhang, S. Mouradian, F. N. C. Wong, and J. H. Shapiro, Phys. Rev. Lett. **114**, 110506 (2015).
[8] Q. Zhuang, Z. Zhang, and J. H. Shapiro, Phys. Rev. Lett. **118**, 040801 (2017).
[9] J. H. Shapiro, Phys. Rev. A **80**, 022320 (2009).
[10] Z. Zhang, M. Tengner, T. Zhong, F. N. C. Wong, and J. H. Shapiro, Phys. Rev. Lett. **111**, 010501 (2013).
[11] S. Barzanjeh, S. Guha, C. Weedbrook, D. Vitali, J. H. Shapiro, and S. Pirandola, Phys. Rev. Lett. **114**, 080503 (2015).
[12] U. Las Heras, R. Di Candia, K. Fedorov, F. Deppe, M. Sanz, and E. Solano, Sci. Rep. **7**, 9333 (2017).
[13] C. W. Helstrom, J. Stat. Phys. **1**, 231 (1969).
[14] A. Chefles, Contemp. Phys. **41**, 401 (2000).
[15] S. M. Barnett and S. Croke, Adv. Opt. Photonics **1**, 238 (2009).
[16] J. Bae and L.-C. Kwek, J. Phys. A: Math. Theor. **48**, 083001 (2015).
[17] K. M. R. Audenaert, J. Calsamiglia, R. Muñoz-Tapia, E. Bagan, Ll. Masanes, A. Acin, and F. Verstraete, Phys. Rev. Lett. **98**, 160501 (2007).

[18] J. Calsamiglia, R. Muñoz-Tapia, L. Masanes, A. Acin, and E. Bagan, Phys. Rev. A **77**, 032311 (2008).
[19] S. Pirandola and S. Lloyd, Phys. Rev. A **78**, 012331 (2008).
[20] M. Nussbaum and A. Szkoła, Ann. Stat. **37**, 1040 (2009).
[21] M. Sanz, U. Las Heras, J. J. García-Ripoll, E. Solano, and R. Di Candia, Phys. Rev. Lett. **118**, 070803 (2017).
[22] M. M. Wilde, M. Tomamichel, S. Lloyd, and M. Berta, Phys. Rev. Lett. **119**, 120501 (2017).
[23] C. Weedbrook, S. Pirandola, J. Thompson, V. Vedral, and M. Gu, New J. Phys. **18**, 043027 (2016).
[24] M. Bradshaw, S. M. Assad, J. Y. Haw, S.-H. Tan, P. K. Lam, and M. Gu, Phys. Rev. A **95**, 022333 (2017).
[25] M. Genovese, J. Opt. **18**, 073002 (2016).
[26] F. Dell'Anno, S. De Siena, L. Albano, and F. Illuminati, Phys. Rev. A **76**, 022301 (2007).
[27] A. Ourjoumtsev, A. Dantan, R. Tualle-Brouri, and P. Grangier, Phys. Rev. Lett. **98**, 030502 (2007).
[28] Y. Yang and F.-L. Li, Phys. Rev. A **80**, 022315 (2009).
[29] H.-J. Kim, J. Kim, and H. Nha, Phys. Rev. A **88**, 032109 (2013).
[30] S. L. Zhang, J. S. Guo, W. S. Bao, J. H. Shi, C. H. Jin, X. B. Zou, and G. C. Guo, Phys. Rev. A **89**, 062309 (2014).
[31] S.-Y. Lee and H. Nha, Phys. Rev. A **82**, 053812 (2010).
[32] S.-Y. Lee, S.-W. Ji, H.-J. Kim, and H. Nha, Phys. Rev. A **84**, 012302 (2011).
[33] H. Ollivier and W. H. Zurek, Phys. Rev. Lett. **88**, 017901 (2001).
[34] L. Henderson and V. Vedral, J. Phys. A: Math. Gen. **34**, 6899 (2001).
[35] S. Ragy, I. R. Berchera, I. P. Degiovanni, S. Olivares, M. G. Paris, G. Adesso, and M. Genovese, J. Opt. Soc. Am. B **31**, 2045 (2014).
[36] S. L. Braunstein and P. Van Loock, Rev. Mod. Phys. **77**, 513 (2005).
[37] C. Weedbrook, S. Pirandola, R. García-Patrón, N. J. Cerf, T. C. Ralph, J. H. Shapiro, and S. Lloyd, Rev. Mod. Phys. **84**, 621 (2012).
[38] J. Johansson, P. Nation, and F. Nori, Comput. Phys. Commun. **183**, 1760 (2012).
[39] J. Johansson, P. Nation, and F. Nori, Comput. Phys. Commun. **184**, 1234 (2013).